Experimental Study of Heat and Mass Transfer from a Horizontal Cylinder in Downward Air-Water Mist Flow with Blockage Effect*

Toshio Aihara
Institute of Fluid Science, Tohoku University, Sendai, Japan

Wu-Shung Fu
Institute of Mechanical Engineering, National Chiao Tung University, Hsinchu, Taiwan, Republic of China

Mitsuo Hongoh
Toshiyuki Shimoyama
Institute of Fluid Science, Tohoku University, Sendai, Japan

■An experimental study was made on convective heat and mass transfer from a horizontal heated cylinder in a downward flow of air-water mist at a blockage ratio of 0.4. The measured local heat transfer coefficients agree fairly well with the authors' numerical solutions obtained previously for the front surface of a cylinder over the ranges mass flow ratio $0–4.5\times10^{-2}$, a temperature difference between the cylinder and air 10–43 K, gas Reynolds number $(7.9–23)\times10^3$, Rosin-Rammler size parameter 105–168 μm, and dispersion parameter 3.4–3.7. Heat transfer augmentation, two-phase to single-phase, of greater than 19 was attained at the forward stagnation point. For heat transfer in the rear part of the cylinder, an empirical formula is derived by taking into account the dimensionless governing variables, that is, coolant-feed and evaporation parameters.

Keywords: *mist flow, two-phase flow, forced convection, heat and mass transfer, heat transfer augmentation*

INTRODUCTION

The cooling of heated bodies by suspending water droplets in a gas stream shows remarkably better heat transfer than single-phase cooling. Accordingly, many theoretical and experimental studies of air-water mist cooling have been carried out. An extensive review of 53 papers was recently made by Aihara [1]. The experimental studies can be divided into two categories.

1. Studies on air-water mist cooling of a smooth circular cylinder (see, eg, Finlay and McMillan [2], Hodgson et al [3], Matsuda et al [4]) and of a bank of tubes (Finlay and McMillan [5], Kuwahara et al [6], Pawlowski and Siwon [7]). Since the heat and mass transfer of air-water mist flow is an extremely complicated phenomenon, the accuracy of the existing experimental values did not satisfactorily verify the validity of the numerical solutions.
2. Studies of heat transfer augmentation using a specially structured surface such as annular roughness, fine grooves, or wire winding (eg, Kosky [8], Kuwahara [9], and Hayashi et al [10]). However, the fact that such fine structures are apt to be covered with a scale of the inorganic substances contained in city/underground water, may present a serious problem in the practical application of these schemes.

We carried out a series of numerical heat/mass transfer analyses [11–13] of the double-boundary layers on a horizontal circular isothermal cylinder in a downward flow of air-water mist of polydisperse droplets, taking into account the droplet trajectories and the blockage effect of the gas-phase flow. In this study, an experiment using an isothermal cylinder with a blockage ratio of $d_c/b = 0.4$ was carried out to verify the validity of our numerical analyses and to derive an empirical formula of heat transfer from the rear half surface of the cylinder to which our theory is inapplicable. This was done to establish the fundamentals of the performance prediction of air-water mist heat exchangers and to obtain the design data.

EXPERIMENTAL APPARATUS AND PROCEDURE

Air-Water Mist Tunnel

Figure 1 illustrates an outline of the wind tunnel used for the present experiment. A blower of the polyvinyl chloride (*1*) was driven by an electric motor whose rotational speed was controlled with an inverter system (*2*). The discharge air flowed into a spray chamber (*4*) of 0.5 m × 0.5 m cross section, through a duct of vinyl chloride (*3*), a constriction duct 78 mm in diameter (*6*), a dry- and wet-bulb temperature-measuring section (*7*), a diffuser with five screens (*8*) [14], and a straightener (*9*). After the temperature was controlled by a water-supply system [15, 16], city water was passed through a pressure controlling valve (*10*) and a temperature-measuring section (*11*); then it was sprayed through hollow-cone spray nozzles in a spray chamber (*4*) and mixed with the air to produce an air-water mist mixture. This binary mixture flowed into a test duct (*13*) of 0.125 m × 0.2 m cross section through a two-stage constriction duct; after passing by a test cylinder (*12*), it was demisted in a U-bend (*14*) and a mist eliminator (*15*). Then the humid air was drawn again into the blower (*1*) through a connection duct with an opening to the ambient air. The 0.125 m side walls of the test duct (*13*) were composed of acrylic resin windows.

*The main part of this paper was originally published in the Japanese language in the *Transactions of the JSME, Ser B*, 53 (492), 2567-2574, 1987.

Address correspondence to Professor T. Aihara, Institute of Fluid Science, Tohoku University, Katahira, Sendai 980, Japan

Experimental Thermal and Fluid Science 1990; 3:623-631

0894-1777/90/$3 50

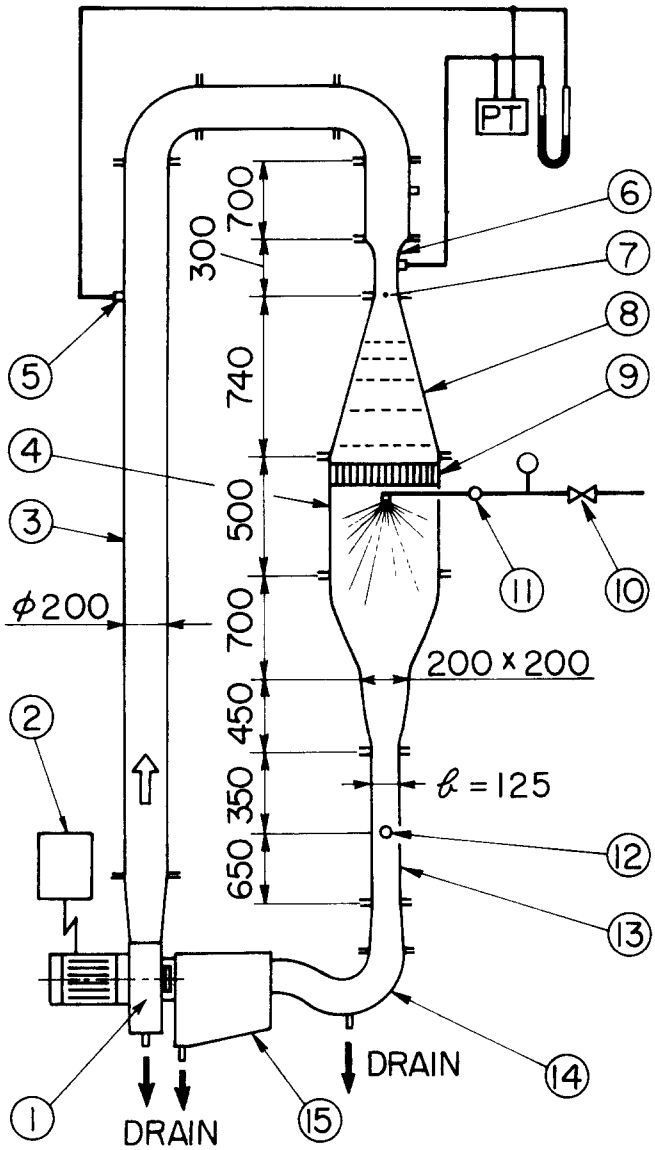

Figure 1. Outline of circulating wind tunnel for air-water mist flow (not to scale; dimensions in mm).

The clear airflow rate and clear air velocity at the channel center of the unobstructed test duct were evaluated by using the calibrated correlations with the static pressure differences between the pressure taps (*5*) and the constriction duct (*6*). The humid airflow rate and its velocity for the air-water mixture were evaluated by applying a density correction to the correlations. The distribution of air velocity at the measuring cross section of the test duct (*13*) was uniform over 85% or more of the channel width b (=0.125 m). Owing to the development of a boundary layer along the duct wall, the gradient of velocity u_c in the flow direction was of the order of 0.2 m/(s m). Pressure was measured with Betz manometers and pressure transducers.

The error in the pressure measurement was ± 0.5 Pa. However, the maximum relative error in determination of the air velocity and flow rate is ± 2.4-3.4% for $u_c \simeq 3$-7 m/s owing to the error for the discharge coefficient of the constriction flowmeter (*6*).

Test Cylinder and Test Duct

A test cylinder with a diameter of 0.05 m and a length of 0.2 m was composed of a test section (*2*) and two guard sections (*3*), as shown in Fig. 2. The cross-sectional view, B in the figure, illustrates the details of the test section (*2*). Twelve copper segments (*2*), having Nichrome heaters (*9*) insulated by porcelain tubes, were bonded and screwed to the bakelite body (*5*). The test section and the guard sections of copper were assembled into one body, and their surface was polished smooth. The guard section was designed to have a length of 49×10^{-3} m, so that most parts of the test section (*2*) could undergo two-dimensional heat transfer [17].

The test cylinder was installed horizontally at the center of the test duct (*13*). Bakelite fin-rings of 63 mm O.D. (*1*) were fitted to both ends of the test cylinder to prevent the water that fell from the duct walls from flowing onto the test cylinder. The local temperatures of the test cylinder were measured with sixty-two 100 μm diameter copper-constantan thermocouples (*6-8*) embedded in the surface To satisfy the condition of uniform wall temperature, the respective electric input to 36 Nichrome heaters (*9*, *10*) was adjusted so that all of the surface temperatures might agree within $\pm 1.6\%$ normally and within $\pm 3\%$ in the worst cases. The outside walls of the test duct were thermally insulated with polyester-isocyanate foam and styrofoam boards, except during the flow observation

The static pressure distribution was measured using a similar cylinder made of a brass block with ten 0.5 mm diameter pressure taps drilled in its surface so as not to interfere with each other.

The measurement of temperatures and pressures and the data reduction were performed by an online system with a data logger and a microcomputer [18]

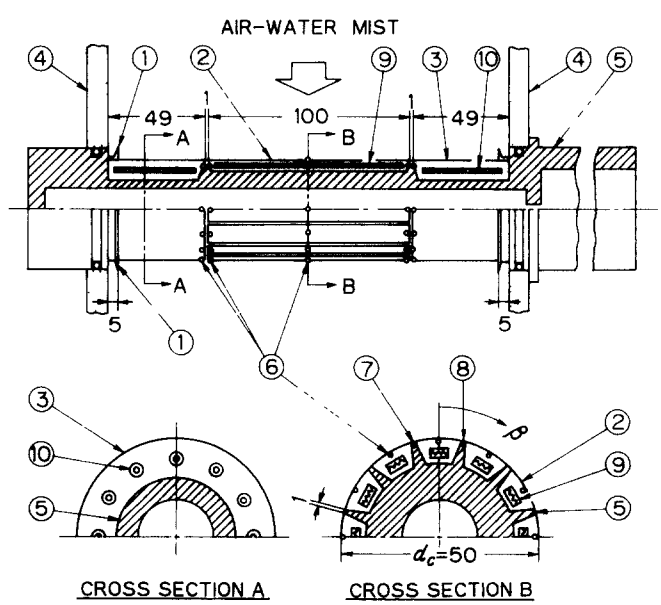

① FIN RING; ② TEST SECTION; ③ GUARD SECTIONS ④ DUCT WALL; ⑤ BAKELITE BODY; ⑥⑦⑧ 0.1-MM-DIA THERMOCOUPLES; ⑨⑩ NICHROME HEATERS

Figure 2. Sectional view of test cylinder (dimensions in mm)

Measurement of Size Distribution and Mass Flow Rate of Suspended Droplets

Water droplets in the main stream were captured at a point 50 mm upstream from the test cylinder with an immersion sampling cell 3 mm × 5 mm each time the experimental conditions were altered. Then the size distribution was measured, allowing for possible error sources such as the shattering of droplets, viscosity of immersion oil, sampling time, and solubility of water droplets in silicone oil [19]. The results can be approximated by the following mass-basis Rosin-Rammler distribution equation within an error of ±4% normally and within ±8% in the worst case.

$$f_{w(d)} = \frac{n}{d_0}\left(\frac{d_p}{d_0}\right)^{n-1} \exp\left[-\left(\frac{d_p}{d_0}\right)^n\right] \quad (1)$$

where $d_0 = 105$–168 μm, $n = 3.4$–3.7, d_p is the droplet diameter, and $f_{w(d)}$ is the size-distribution function.

The mass flow rate of water droplets was measured on each run by isokinetic sampling with a collection probe, as shown in Fig. 3, within an error of ±1%. The collection probe was a glass tube with an inner diameter of 8 mm and a thickness of 1 mm. Four trial probes having different bend shapes were tested for air–water separation performance; then the best dimensions of the bend were determined as the radius $r = 10$ mm and inside diameter $a = 5$ mm. To prevent the condensation of dew in the rotor meter for measuring the airflow rate, a heating section was joined to the meter upstream to be used as needed. Other measuring procedures were substantially the same as described in the previous report [16]. The probe hole in the duct wall was closed completely with a blind plug before each heat transfer experiment.

Measurement of Dry- and Wet-Bulb Temperatures and Humidity

After complete demisting by the air–water separator shown in Fig. 3, the dry- and wet-bulb temperatures of the humid air were measured with the specially designed thermometers,

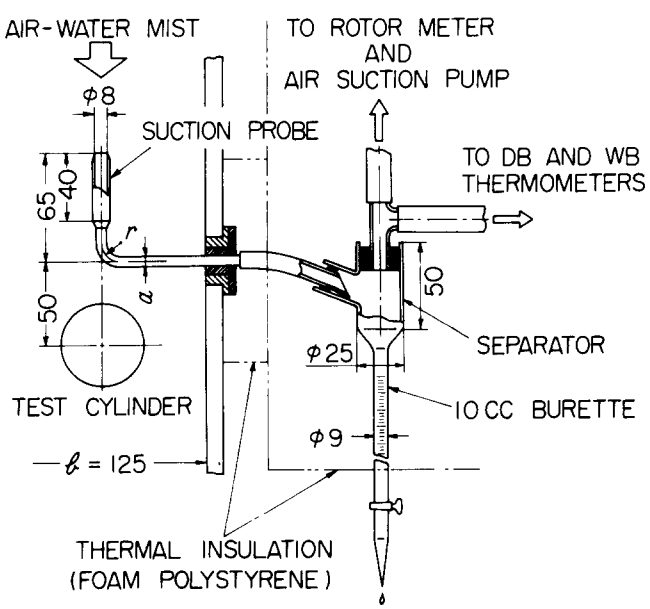

Figure 3. Collection probe for measuring mass flow rate of water droplets (not to scale).

the details of which are given in Ref. [16]. The thermometers, separator, and connecting line of polyvinyl chloride tube were fully thermally insulated to prevent dew condensation in the measuring system. The absolute humidity χ of the air–water mist flow through the test duct was determined from the measured dry- and wet-bulb temperatures.

The wet-bulb temperature T_g' of the air–water mist flow was measured with the exposed 100 μm diameter copper-constantan thermocouples, which were located at two points, 0.17 m upstream of the test cylinder and 59 mm from the duct centerline toward each duct wall (*4*) in Fig. 2. The relative humidity and dry-bulb temperature T_g of the air–water mist flow were determined from the values of χ and T_g'. The error in the measurement of T_g and T_g' was ±0.2 K. This measuring method was adopted because the distribution of T_g' was uniform throughout the measuring cross section of the test duct and the relative humidity was 98% or higher for most runs.

Determination of Heat Transfer Coefficients

The average heat transfer coefficient h over the interval $\Delta\beta = \pi/6$ rad for a heat transfer segment of the test cylinder is defined by Eq. (2), regardless of whether it is single- or two-phase, for $T_g \cong T_g'$. Hereinafter this is referred to as the local heat transfer coefficient.

$$h = Q_j/(T_{w,j} - T_g)(A + A^* f) \quad (2)$$

Here $T_{w,j}$ and A are the average surface temperature and heat transfer area, respectively, of the jth segment from the stagnation point; A^* is one-half of the exposed area of the bakelite fins surrounding the segment (cf. *5* in cross section B of Fig. 2); and f is the correction factor for thermal resistance through the bakelite fins, given by

$$f = (T_{w,j}^* - T_g)/(T_{w,j} - T_g) \quad (3)$$

where $T_{w,j}^*$ is the average tip temperature of the bakelite fins surrounding the jth segment (cf. *7* and *8* in Fig. 2).

The numerator of Eq. (2), $\dot{Q}_j$, is the rate of convective heat transfer from the jth segment, which is determined by subtracting the radiative heat transfer rate $\dot{Q}_{r,j}$ of Eq. (4) from the net electric input after correcting for the internal resistance of electric measuring instruments and the heat leakage through the current leads.

$$\dot{Q}_{r,j} \cong \sigma\epsilon A(T_{w,j}^4 - T_e^4) + \sigma\epsilon^* A^*(T_{w,j}^{*4} - T_e^4) \quad (4)$$

where σ is the Stefan-Boltzmann constant; T_e the duct wall temperature; ϵ the emissivity of the segment surface, estimated as $\epsilon \cong 0.1$ for a clear polished, but somewhat oxidized, copper surface; and ϵ^* the emissivity of a polished bakelite surface, estimated as $\epsilon^* \cong 0.9$. Furthermore, the geometrical factor is assumed to be unity in Eq. (4).

The error in measurement of the temperature $T_{w,j}$ was ±0.1 K. The electrical input power was measured with analog ammeters and a digital voltmeter; the experimental error for $\dot{Q}_j$ is predicted to be of the order of ±1.4%. Consequently, the maximum indeterminate error for the local heat transfer coefficient h, amounts to ±5%.

RESULTS AND DISCUSSION

Experiment on Single-Phase Flow

An experiment was carried out on clear airflow to verify the accuracy of the present experiment and to obtain the data for $M = 0$.

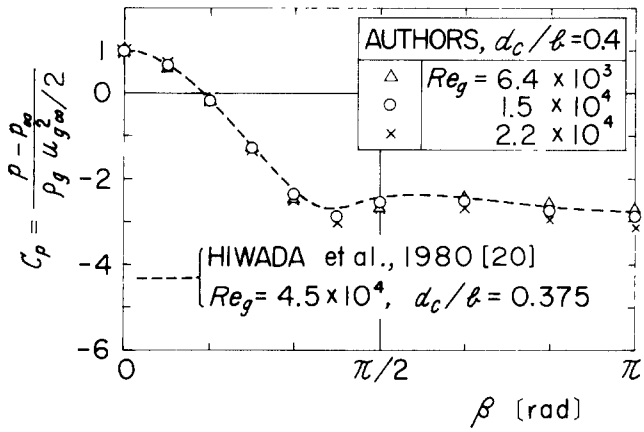

Figure 4. Distribution of pressure coefficient C_p around a cylinder in clear airflow

Free-Stream Turbulence and Pressure Distribution Around a Cylinder The intensity of free-stream turbulence Tu $(=\sqrt{u'^2}/u)$ was measured by a hot-wire anemometer at a distance 0.14 m upstream from the test cylinder. The measurement indicated that Tu = 1 ± 0.3% for the central 70% of the channel width b (=0.125 m) for u_c = 3–7 m/s. This turbulence can be attributed to the wake from the spray system existing upstream.

Figure 4 shows a comparison of our measured values of the pressure coefficient C_p around the cylinder with the data obtained by Hiwada and Mabuchi [20] under similar conditions. The agreement is very good.

Single-Phase Heat Transfer Coefficients Figure 5 is a plot of the local Nusselt number $Nu_{(l)}$ $(\equiv h_{(l)}d_c/\lambda_g)$ for clear air against the azimuth angle β from the stagnation point. Here the fluid physical properties are evaluated at the film temperature, the separation angle β_s is considered to be about 1.5 rad on the basis of Hiwada et al's experimental result [21], and the measured values for the separated region are plotted in the form of $Nu_{(l)}/Re_g^{2/3}$, following the method of Hiwada et al [21] and Igarashi and Hirata [22].

In Fig. 5, the data of Hiwada et al [21] on the Sherwood number Sh were converted into the local Nusselt numbers by applying the heat-mass transfer analogy

$$Nu_{(l)} = (Pr/Sc)^n Sh \tag{5}$$

where Pr and Sc are the Prandtl and Schmidt numbers, respectively, and the values of n = 0.37 and Sc = 2.54 for sublimation of naphthalene in air are adopted with reference to the data of Zukauskas [23] and Hiwada et al [21] Our measured values agree very well with those of Hiwada et al. Furthermore, it can be seen in Fig. 5 that the numerical solutions obtained by Aihara et al [13] are in good agreement with the present experimental values for the region of $\beta < 1.2$ rad, which is important in air–water mist heat transfer

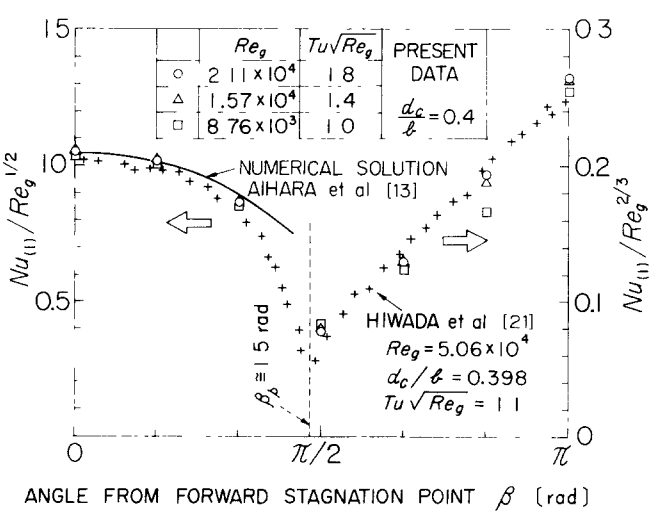

Figure 5. Local Nusselt number $Nu_{(l)}$ for clear airflow (M = 0).

The present experimental data on the average Nusselt number $\overline{Nu}_{re,(l)}$ for the surface of the rear half of the cylinder $[\beta/\pi = 0.5\text{–}1]$ are correlated well with

$$\overline{Nu}_{re,(l)} = 0.161\ Re_g^{2/3} \tag{6}$$

The numerical solutions of Ref. 13 for the Nusselt number of the forward stagnation point, $Nu_{0,(l)}$, can be approximated by

$$Nu_{0,(l)} = 1.05\ Re_g^{1/2} \tag{7}$$

Therefore, the following empirical formula is derived for $d_c/b = 0.4$·

$$(\overline{Nu}_{re}/Nu_0)_{(l)} = 0.153\ Re_g^{1/6} \tag{8}$$

On the other hand, the experimental data of Hiwada et al. [21] on the average heat transfer coefficient for the separated region can be correlated with the following equation within an error of ± 1%:

$$\left(\frac{\overline{Nu}_{re}}{Nu_0}\right)_{(l)} = 0.130\left[1 + 1.1\left(\frac{d_c}{b}\right)^2\right] Re_g^{1/6} \tag{9}$$

The present empirical equation, Eq. (8), shows good agreement with Eq. (9) with d_c/b = 0.4. This indicates that the present experiment was accurate.

Experiment of Air–Water Mist Flow

The experiment was carried out for an air velocity u_c = 3–7 m/s, gas Reynolds number Re_g = 8 × 10^3–2.3 × 10^4, temperature difference ΔT_w $(=T_w - T_g) \cong$ 10–43 K, mass flow ratio M = (2.6–4.5) × 10^{-2}, and a relative humidity of air of 98% or higher for most runs. According to observations with the naked eye, water droplets travel in nearly vertical and straight paths because the comparatively long straight duct was arranged upstream from the test cylinder. The horizontal distribution of the mass flow rate of water droplets G_p was within + 6 to − 3% in the vicinity of the test section of the cylinder, although it was within about ± 20% throughout the cross section of the test duct.

After continuous running for many hours as a preliminary heat transfer experiment on water–air mist flow, the surface of the test cylinder was polished smooth again to avoid obstruction of the flow of water film on the surface caused by the swelling of the tips of the bakelite fins (cf. (5) in Fig. 2). Then the main experiment was carried out.

Size Distribution of Water Droplets Figure 6 shows a typical plot of the measured size distributions on Rosin-Rammler paper in the form of the mass basis cumulative oversize fraction R_w. The figure shows that the suspended droplets had a

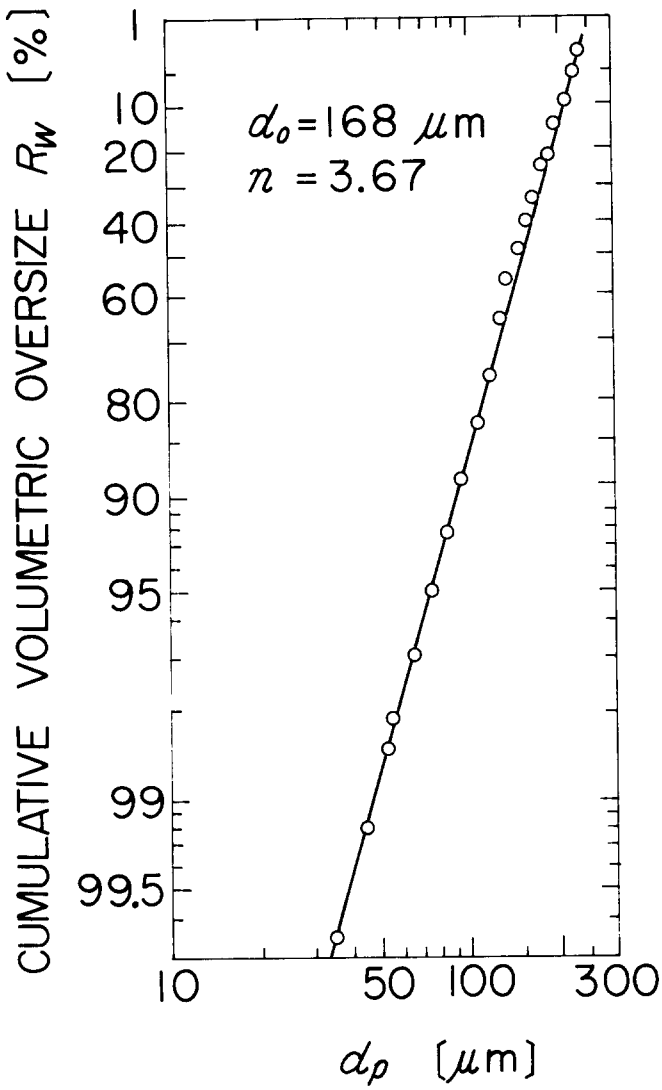

Figure 6. Typical droplet-size distribution for $u_c = 2.8$ m/s and a spray pressure of 0.29 MPa.

clear Rosin-Rammler distribution. The droplet size distribution was measured at each run, since it depends on the air velocity u_c.

Water Film Formation A continuous, thin water film was formed on the surface of the front half of the test cylinder owing to droplet impingement, as expected from the theoretical predictions [13]. This can be attributed to the fact that the gas-phase flow separation has a slight influence on the droplet collection efficiency of the cylinder [11] and that the free-stream turbulence of an intensity as measured in the present experiment has little effect on the drag coefficient for droplets [24].

The state of wetting on the surface of the rear half of the cylinder varies with time as follows. At the initial stage when the cylinder surface was just polished, the water falling from the front half of the cylinder broke up into many unstable ligaments at $\beta \cong \pi/2$ and then fell in drops at the backward stagnation point. After the preliminary running for several dozen hours, a major portion of the cylinder surface was covered with a scale film about 10 μm thick. Hence, distinct stable

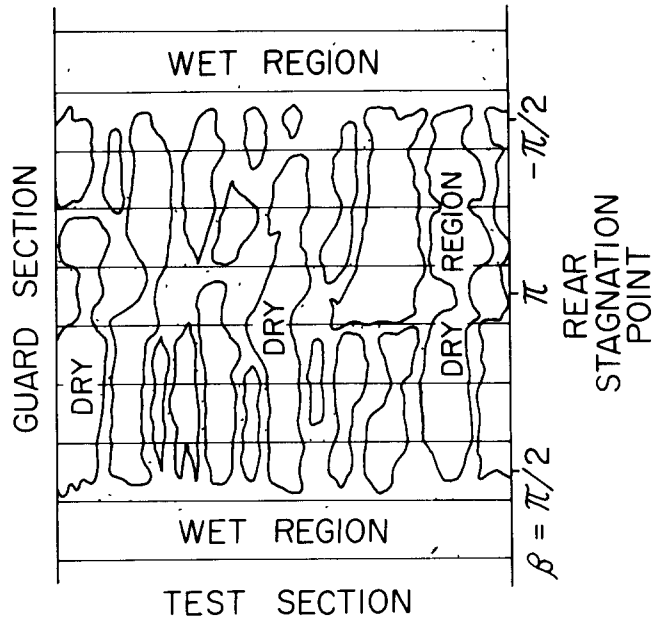

Figure 7. Sketch of water film on the surface of the rear half of a cylinder ($\Phi_w = 2.5$–2.9).

paths of water were formed, as shown in Fig. 7, while the dry area of the cylinder surface was slightly oxidized. Partial breakup of the water film was observed even at the location of $\beta \cong 1.5$ rad, corresponding to the separation point in a clear airflow. In the case shown in Fig. 7, the ratio of the wetted area to the heat transfer area downstream from the separation point, ξ, reached 0.63.

Local Heat Transfer Coefficients Figures 8 and 9 are

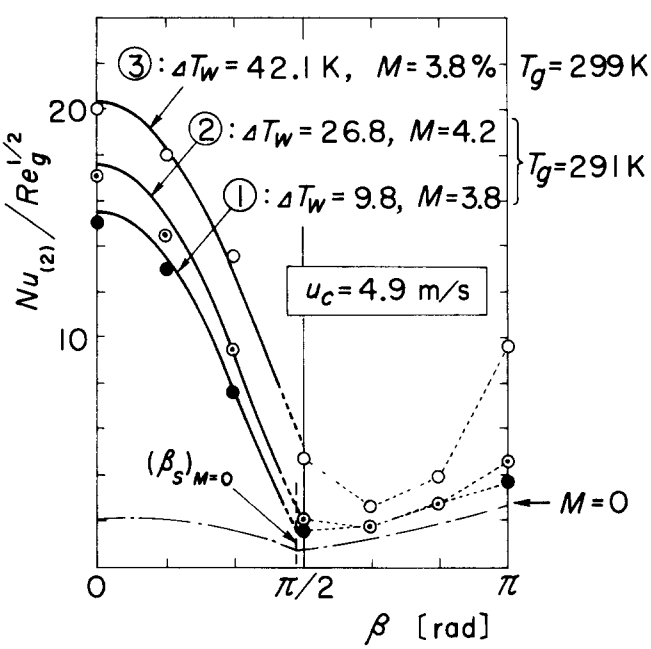

Figure 8. Comparison of local Nusselt number $Nu_{(2)}$ for air–water mist flow between the present experimental data and the numerical solutions by Aihara et al [13] for $Re_g = (1.38\text{–}1.62) \times 10^4$ and $d_c/b = 0.4$; $d_0 = 142$ μm and $n = 3.7$ for curves 1 and 2; $d_0 = 108$ μm and $n = 3.4$ for curve 3.

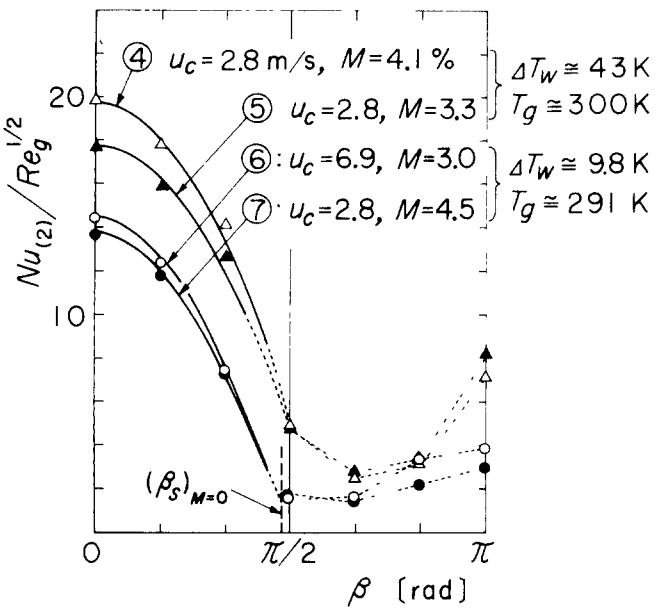

Figure 9. Comparison of local Nusselt number $Nu_{(2)}$ between the present experimental data and the numerical solutions by Aihara et al [13] for $Re_g = (0.8\text{–}2.2) \times 10^4$ and $d_c/b = 0.4$; $d_0 = 168$ μm and $n = 3.7$ for curve 4; $d_0 = 111$ μm and $n = 3.4$ for curve 5; $d_0 = 120$ μm and $n = 3.7$ for curve 6, $d_0 = 168$ μm and $n = 3.7$ for curve 7.

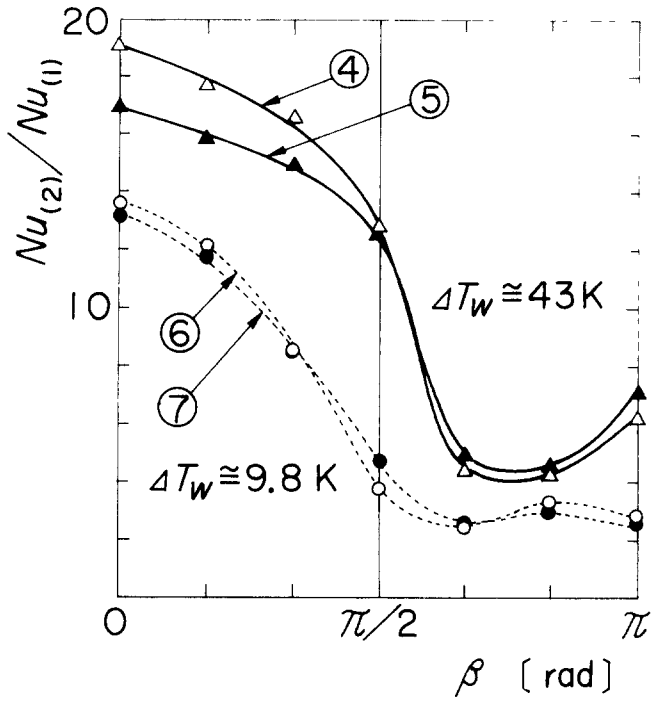

Figure 10. Effect of temperature difference ΔT_w $(= T_w - T_g)$ on distribution of local enhancement factor $Nu_{(2)}/Nu_{(1)}$, other parameters and symbols are the same as in Figs. 8 and 9.

typical plots of the measured local Nusselt number, $Nu_{(2)}$ $(\equiv h_{(2)}d_c/\lambda_g)$, in which the physical properties of humid air [25] are evaluated at the film temperature and film humidity $\chi_f = (\chi_w + \chi_g)/2$. The numerical solutions of Aihara et al [13], the solid lines in Figs. 8 and 9, are in very good agreement with the present experimental data, and the lines of their extrapolation almost agree with the measured values for $\beta = \pi/2$.

There are considerable differences in the distribution of the local Nusselt number in the rear half of the cylinder between the clear airflow and the air–water mist flow. In the separated region of clear airflow, a reverse flow creeps up from the backward stagnation point of the cylinder toward the separation point; as a consequence, the local Nusselt number $Nu_{(1)}$ increases greatly with β. In contrast to this, the local Nusselt number $Nu_{(2)}$ for the air–water mist flow takes a minimum value at $\beta \cong 2\pi/3$ in the case of a large temperature difference, whereas it gradually increases with β in the case of a small temperature difference. The reasons for this are that the water film on the cylinder has the antipodal characteristics of evaporative cooling and thermal resistance and the wet-area fraction ξ varies according to the governing parameters Λ and Φ described later.

Generally speaking, the smaller the temperature difference ΔT_w and the greater the mass flow ratio M, the thicker the water film near the backward stagnation point. This prevents an increase in $Nu_{(2)}$ in the case of small ΔT_w, where evaporative cooling is weak. In the case of large ΔT_w, where the evaporative cooling is active, the value of $Nu_{(2)}$ decreases once with β because of a sudden decrease in ξ on β exceeding $\pi/2$; then $Nu_{(2)}$ increases greatly on approaching the backward stagnation point, owing to the sufficient water quantity near the bottom of the cylinder, the cooling of air by droplet evaporation in the reverse-flow region, and the low thermal resistance across the thin branch streams.

The local enhancement factors of heat transfer, $Nu_{(2)}/Nu_{(1)}$, are plotted in Fig. 10, where the heat transfer mechanisms can be seen more clearly. In the present experiment, heat transfer enhancement exceeding a factor of 19 was attained.

Empirical Formula of Heat Transfer Coefficient for the Rear Half of a Cylinder It can be seen from the above that a numerical analysis of heat and mass transfer from the rear half of the cylinder would be much too complicated, although detailed numerical analysis has almost been completed for the front half. Hence, an empirical formula will be more practical for the prediction of heat transfer from the rear half of the cylinder.

On the basis of the theoretical analyses by Aihara et al [11–13, 16], the following approximate relation can be derived:

$$\left(\frac{\overline{Nu}_{re}}{Nu_0}\right)_{(2)} \cong \left(\frac{\overline{Nu}_{re}}{Nu_0}\right)_{(1)} \frac{(1-\xi_e)+\xi_e(1+\Phi_w)}{\left[1+\Phi_w\left(\frac{Pr}{Sc}\right)^{2/3}\right]+\Lambda\eta_0\dfrac{Re_g^{1/2}}{Nu_{0,(1)}}} \tag{10}$$

where $\overline{Nu}_{re,(2)}$ is the average Nusselt number for the rear half $[\beta/\pi = 0.5\text{–}1]$ of the cylinder in an air–water mist flow, $Nu_{0,(2)}$ is the local Nusselt number for its forward stagnation point, η_0 is the local total collection efficiency, Pr and Sc are the Prandtl and Schmidt numbers of humid air, respectively, and ξ_e is the effective wet-area fraction for the rear half of the cylinder, allowing for the temperature drop across the water film of branch streams. Here η_0 is a function of Re_g,

n, d_c/b, and d_0/d_c and ξ_e is a function of the coolant-feed parameter Λ and evaporation parameter Φ_w, defined as

$$\Lambda = M \,\mathrm{Pr}\, \mathrm{Re}_g^{1/2}(c_l/c_g) \tag{11}$$

$$\Phi_w = \frac{(\chi_w - \chi_g) r_w}{(T_w - T_g) c_g} \tag{12}$$

where c_l and c_g are the specific heat at constant pressure of water and humid air, respectively, and χ_w and r_w are the saturated absolute humidity and the latent heat of evaporation of water at a temperature T_w. Therefore, substituting Eq. (9) into Eq. (10) gives the expression

$$\left(\frac{\overline{\mathrm{Nu}}_{\mathrm{re}}}{\mathrm{Nu}_0}\right)_{(2)} \frac{1}{\mathrm{Re}_g^{1/6}} = \text{function of } \Lambda, \Phi_w, \mathrm{Re}_g, \frac{d_c}{b}, \frac{d_0}{d_c}, n \tag{13}$$

The relationship of the main relevant parameters to the left-hand side of Eq. (13) are shown in Fig. 11.

As can be seen from the figure, the dimensionless term $(\overline{\mathrm{Nu}}_{\mathrm{re}}/\mathrm{Nu}_0)_{(2)}\mathrm{Re}_g^{-1/6}$ can be correlated approximately with Λ alone within the experimental ranges, although there are slight differences depending on d_0 or $\bar{d}_p$, n, Φ_w, and the properties of the heat transfer surface. This suggests that the effects of Φ_w, Re_g, d_c/b, d_0/d_c, and n may offset each other by taking the form $(\overline{\mathrm{Nu}}_{\mathrm{re}}/\mathrm{Nu}_0)_{(2)}$. Then the following empirical formula is derived from the data in Fig. 11, excluding the data of Hodgson et al [3] for the low Reynolds number:

$$\overline{\mathrm{Nu}}_{\mathrm{re},(2)} = 0.093\, \mathrm{Nu}_{0,(2)}\, \mathrm{Re}_g^{1/6}/\Lambda^{1/3} \tag{14}$$

PRACTICAL USEFULNESS/SIGNIFICANCE

Several closed-form empirical formulas for the average Nusselt number for the front half or whole surface of a circular cylinder in an air–water mist flow have been presented in the literature (eg, Refs. 2, 8, 26). In these formulas, the average Nusselt number is given simply as a function of Re_g, M, and β. However, as may be seen from the detailed numerical analysis by Aihara et al [13], the average Nusselt number is indeed a function of Re_g, M, d_c/b, Froude number (Fr), T_w and T_g, χ_w and χ_∞, (d_0/d_c), n, $d_{\max}/d_0$, $d_{\min}/d_0$, all physical properties of both fluids, and their temperature dependence. The local Nusselt number depends further on the azimuth angle β. Therefore, as for the Nusselt number for the front half of a cylinder, we recommend the use of the numerical results of Ref. 13, which have been shown to agree very well with the experimental data in this report.

The average Nusselt number for the rear half of the cylinder, $\overline{\mathrm{Nu}}_{\mathrm{re},(2)}$, can be predicted by using Eq. (14), within an error of $\pm 20\%$ over the ranges $d_c/b = 0.1$–0.4, $\mathrm{Re}_g = 4 \times 10^3$–$1.2 \times 10^5$, $\Lambda = 2$–70, and $\Phi_w = 2.5$–10.4, regardless of the surface wettability of the cylinders tested, as shown in Fig. 11. This accuracy is sufficient in practice, because the value of $\overline{\mathrm{Nu}}_{\mathrm{re},(2)}$ is generally around one-fourth of the average Nusselt number for the front half. The procedure for predicting $\overline{\mathrm{Nu}}_{\mathrm{re},(2)}$ is as follows.

Specification for an Exercise $\mathrm{Re}_g = 1.7 \times 10^4$, $d_c/b = 0.4$, $d_0/d_c = 2 \times 10^{-3}$, $d_{\min} = 99.9\%$ diameter (oversize), $d_{\max} = 1\%$ diameter, $n = 3$, $M = 10^{-2}$, $\Delta T_w = 30$ K, $T_g = 283$ K, and relative humidity = 100%.

Evaluation of $\mathrm{Nu}_{0,(2)}$ From the numerical solutions presented by Aihara et al [13], the stagnation-point Nusselt number of a cylinder in a downward flow of air–water mist under $g = 9.8\ \mathrm{m/s^2}$ is determined to be $\mathrm{Nu}_{0,(2)} = 7.7\sqrt{\mathrm{Re}_g} = 1004$ for the above specification.

We can also evaluate the approximation value of $\mathrm{Nu}_{0,(2)}$ as follows. First, the stagnation-point Nusselt number for single-phase airflow is calculated to be $\mathrm{Nu}_{0,(1)} = 136$ with Hiwada and Mabuchi's empirical formula [20], the error of which is $\pm 5\%$ for $\mathrm{Re}_g = 10^4$–10^5 and $d_c/b = 0$–0.8.

$$\mathrm{Nu}_{0,(1)} = 0.960\,\mathrm{Re}_g^{0.5}\left[1 + 1.03\left(\frac{d_c}{b}\right)^2 + 1.09\left(\frac{d_c}{b}\right)^3 - 1.84\left(\frac{d_c}{b}\right)^4\right]^{0.5} \tag{15}$$

Then the equivalent droplet diameter d_e and stagnation-point collection efficiency η_0 for the air–water mixture described above are determined to be $d_e/d_c = 1.58 \times 10^{-3}$ and $\eta_0 = 0.825$ using the following correlations derived by Aihara et al [12, 13].

$$\frac{d_e}{d_c} = 0.196\left(\frac{d_0}{d_c}\right)^p n^{1.17}\,\mathrm{Re}_g^{-0.057} \cdot \left[1 - 0.04\left(\frac{d_c}{b} + \frac{1}{\mathrm{Fr}}\right)\right] \tag{16}$$

with

$$p = 0.73 n^{0.18}$$

$$\eta_0 = \left(1 - \frac{1}{K^*}\right)\left[1 + \frac{3.8}{\mathrm{Re}_p^{0.88}}\left(\frac{d_c}{b}\right)^{1.5}\right] \cdot \left[1 + \frac{0.72}{(\mathrm{Re}_p\,\mathrm{Fr})^{0.78}}\right] \tag{17}$$

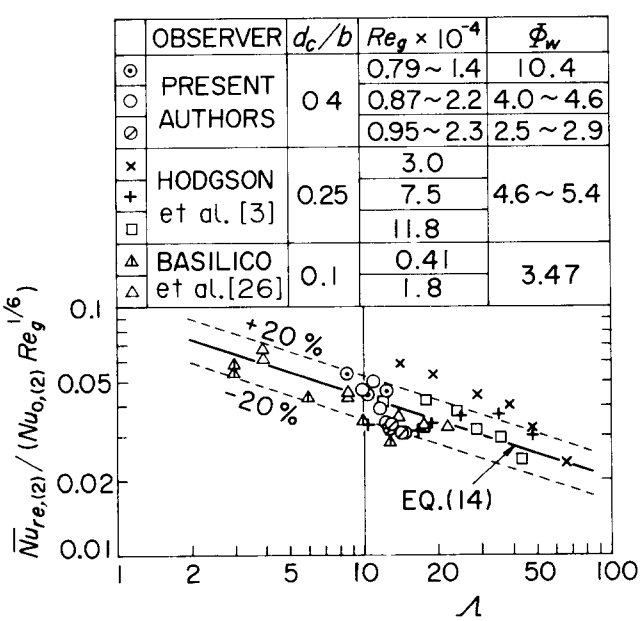

Figure 11. Average Nusselt number $\overline{\mathrm{Nu}}_{\mathrm{re},(2)}$ for the rear half of a cylinder. Present data: $d_c = 0.05$ m, $d_0 = 105$–168 μm, $n = 3.4$–3.7. Hodgson et al [3]: $d_c = 0.076$ m, $\bar{d}_p = 114$–305 μm, $n \cong 1.8$. Basilico et al [26]: $d_c = 0.02$ m, $(\bar{d}_p)_{\mathrm{sauter}} = 9.25$ μm, $n \cong 7$.

with

$$K^* = 2.99 \exp\{0.054(\ln K + 10.2) \ln K\} \quad (18)$$

where Re_p and Fr are the droplet free-stream Reynolds number and Froude number, respectively,

$$Re_p = Re_g(d_e/d_c) \quad (19)$$

$$Fr = u_g/(gd_c)^{1/2} \quad (20)$$

and K is the inertia parameter, defined as

$$K = \frac{1}{18}\left(\frac{d_e}{d_c}\right)^2 \left(\frac{\rho_p}{\rho_g}\right) Re_g \quad (21)$$

Since $\Lambda_f = 3.67$ for the given specification, the front half of the cylinder can be assumed to be completely wetted [16, 27]. Therefore, empirical formula (14) and the following approximate expression [27] for $Nu_{0,(2)}$ are applicable.

$$Nu_{0,(2)} \cong Nu_{0,(1)}\Theta_0[1 + (Pr_g/Sc_g)^{2/3}\Phi_t] + Re_g^{0.5}\eta_0\Theta_0\Lambda_f \quad (22)$$

where Pr and Sc are the Prandtl and Schmidt numbers, respectively, of humid air, and the subscripts i and f refer to the corresponding conditions to the gas–liquid interface and the film temperature and film humidity, respectively. The temperature ratio Θ was given by Aihara et al [28], within an error of $\pm 2\%$, as

$$\Theta \equiv (T_i - T_g)/(T_w - T_g) = 1 - (2.8 \times 10^{-3})\left(\frac{d_0}{d_c}\right)^{0.33} \cdot (M\,Re_g)^{0.83}\left[1 - \left(\frac{2\beta}{\pi}\right)^2\right] \quad (23)$$

We obtain $\Phi_t = 3.02$ and $\Theta_0 = 0.97$ for the given specifications. Hence, the approximate value of $Nu_{0,(2)}$ is determined to be 961 using Eq. (22) with $Pr_g = 0.71$ and $Sc_g = 0.6$. It is a matter of course that the approximate value of the local Nusselt number $Nu_{(2)}$ at any other azimuth angle β can be also evaluated by a procedure [27] similar to the one mentioned above.

Prediction of $\overline{Nu}_{re,(2)}$ Finally, using Eq. (14), the average Nusselt number for the rear half of the cylinder is determined to be

$\overline{Nu}_{re,(2)} = 307$ from numerical solution of $Nu_{0,(2)} = 1004$

or

$\overline{Nu}_{re,(2)} = 294$ from approximate value of $Nu_{0,(2)} = 961$

CONCLUSIONS

An experiment on heat and mass transfer from a horizontal circular cylinder with uniform surface temperatures in a downward flow of air–water mist at a blockage ratio of 0.4 was carried out. The results obtained are summarized as follows.

1. All measured values of the local heat transfer coefficient for a clear airflow ($M = 0$) agree very well with the previous experimental results. Furthermore, those for the front half ($\beta = 0$–$\pi/2$ rad) of a cylinder agree well with the numerical solutions obtained previous by us.
2. The experimental data on the local heat transfer coefficient for the front half of a cylinder in an air–water mist flow agree well with our numerical solutions and the extrapolation from them; hence, the validity of our solutions has been verified. The maximum heat transfer enhancement in the present experiment is increased 19-fold or more at the forward stagnation point for $M = 4\%$.
3. The thin water film formed on the front half of the cylinder by droplet impingement breaks up into many branch streams near the location of $\beta \cong 1.5$ rad, corresponding to the separation point in a clear airflow; the wet-area fraction of the rear-half surface reaches 0.63
4. The distribution of the local heat transfer coefficient in the rear half of the cylinder differs markedly from that for a clear airflow, owing to the various effects of the wet-area fraction, the thermal resistance of the water film, and the gas-phase cooling in the reverse-flow region. In the case of a large temperature difference, the local heat transfer coefficient takes a minimum value at $\beta \cong 2\pi/3$.
5. A simple empirical formula of the average Nusselt number for the rear half of the cylinder has been derived as a function of the Nusselt number for the forward stagnation point, gas Reynolds number, and coolant-feed parameter

This work is part of the research project carried out with Grant-in-Aid for Scientific Research B-58460105 from the Ministry of Education, Science and Culture of Japan

NOMENCLATURE

A	heat transfer area, m^2
b	channel width, m
c	specific heat at constant pressure, kJ/(kg·K)
d_c	diameter of circular cylinder, m
d_p	diameter of droplet, μm
d_0	size parameter in Rosin-Rammler equation, Eq. (1), μm
G_p	mass flow rate of droplets far upstream, kg/(m^2·s)
h	local heat transfer coefficient, Eq. (2), W/(m^2·K)
$\bar{h}_{re}$	average heat transfer coefficient of rear half surface for $\beta = (\pi/2)$–π rad, W/(m^2·K)
M	liquid/gas mass flow ratio ($=G_p/u_c\rho_g$), dimensionless
n	dispersion parameter in Rosin-Rammler equation, Eq. (1), dimensionless
Nu	local Nusselt number ($=hd_c/\lambda_g$), dimensionless
Q	heat transfer rate, W
r	latent heat of evaporation, kJ/kg
Re_g	gas Reynolds number ($=d_c u_c/\nu_g$), dimensionless
T	temperature, K
T'	wet-bulb temperature, K
ΔT_w	$T_w - T_g$, K
u_c	air velocity at the center of test channel without a heated cylinder, m/s

Greek Symbols

β	azimuth angle from the forward stagnation point, rad
λ	thermal conductivity, W/(m·K)
ν	kinematic viscosity, m^2/s
ξ	wet-area fraction, defined as the percentage of total heat transfer area covered by a liquid film, dimensionless

ρ density, kg/m^3
χ absolute humidity of air, kg/kg (dry)
Λ coolant-feed parameter, Eq. (11), dimensionless
Φ evaporation parameter, Eq. (12), dimensionless

Subscripts

g gas phase or humid air
l liquid film
re rear half of cylinder
w heated wall
0 forward stagnation point
(1) clear airflow
(2) air-water mist flow

REFERENCES

1. Aihara, T., Heat Transfer Augmentation by Gas-Liquid Mist Flow for Thermal Control (Keynote Paper), *Proceedings,* Third International Symposium on Transport Phenomena in Thermal Control, Taipei, pp. 449-464, Aug. 1988
2. Finlay, I. C., and McMillan, T., Heat Transfer During Two-Component Mist Flow Across a Heated Cylinder, *Proc. Inst. Mech Eng*, **182**(3H), 277-288, 1967/1968.
3. Hodgson, J. W., Saterbak, R T., and Sunderland, J. E., An Experimental Investigation of Heat Transfer from a Spray Cooled Isothermal Cylinder, *J Heat Transfer,* **90**, 457-463, 1968
4 Matsuda, O , Takimoto, A., and Hayashi, Y , Study on Mist Cooling for Heat Exchangers (Mist-cooled heat transfer from a circular tube in a horizontal spray flow), *Trans Jpn Soc Mech. Eng (Ser B),* **54**, 2864-2871, 1988 (in Japanese).
5 Finlay, I. C., and McMillan, T , Pressure Drop, Heat and Mass Transfer During Air/Water Mist Flow Across a Bank of Tubes, NEL-Report No. 474, 1970
6. Kuwahara, H., Hirasawa, S , Nakayama, W , and Mori, Y , Heat Transfer from Mist-Cooled Tube Bundles, *Trans Jpn Soc Mech Eng. (Ser B),* **50**, 1549-1557, 1984 (in Japanese)
7. Pawlowski, M., and Siwon, B., Heat Transfer Between Gas-Liquid Spray Stream Flowing Perpendicularly to the Row of the Cylinders, *Warme-Stoffübertrag.,* **22**, 97-109, 1988.
8. Kosky, P G., Heat Transfer to Saturated Mist Flowing Normally to a Heated Cylinder, *Int J Heat Mass Transfer,* **19**, 539-543, 1976
9. Kuwahara, H , Nakayama, W., and Mori, Y., Heat Transfer from the Heated Cylinders Provided with Surface Structures to Air/Water Flows, *Trans Jpn Soc Mech Eng. (Ser B),* **47**, 326-335, 1981 (in Japanese)
10 Hayashi, Y , Takimoto, A., Matsuda, O , and Kitagawa, T., Study on Mist Cooling for Heat Exchangers (Development of high-performance mist cooled heat transfer tubes), *Trans Jpn Soc Mech Eng (Ser B),* **54**, 2617-2623, 1988 (in Japanese).
11 Aihara, T , and Fu, W.-S., Effect of Droplet-Size Distribution and Gas-Phase Flow Separation upon Inertia Collection of Droplets by Bluff Bodies in Gas-Liquid Mist Flow, *Int J Multiphase Flow,* **12**, 389-403, 1986.
12. Aihara, T., Fu, W -S., and Suzuki, Y., Effects of Droplet-Size Distribution and Flow-Blockage upon Inertia Collection of Droplets by Horizontal Cylinders in Downward Flow of Gas-Liquid Mist, *Proceedings,* Japan-U.S. Seminar on Two-Phase Flow Dynamics, Ohtsu, pp. D.1-1 to D 1-9, July 1988
13. Aihara, T., Fu, W.-S., and Suzuki, Y., Numerical Analysis of Heat and Mass Transfer from Horizontal Cylinders in Downward Flow of Air-Water Mist, *J. Heat Transfer,* **112**, 472-478, 1990.
14. Mehta, R. D., The Design of Wide-Angle Diffusers, Imperial College of Science and Technology, Dept. of Aeronautics, I.C Aero Report 76-03, 1976.
15. Aihara, T., and Taga, M , Structure and Performance of a Wind Tunnel for Air-Water Mist Flows, *Mem Inst High Speed Mech , Tohoku Univ ,* **38**, 23-34, 1976 (in Japanese)
16. Aihara, T , Taga, M., and Haraguchi, M , Heat Transfer from a Uniform Heat Flux Wedge in Air-Water Mist Flows, *Int. J. Heat Mass Transfer,* **22**, 51-60, 1979.
17. Goldstein, R. J., and Karni, J., The Effect of a Wall Boundary Layer on Local Mass Transfer from a Cylinder in Cross-Flow, *J Heat Transfer,* **106**, 260-267, 1984.
18. Aihara, T , Maruyama, S , Hongoh, M , and Aya, S , Heat Transfer and Pressure Loss of a Very Shallow Fluidized-Bed Heat Exchanger. 1 Experiment with a Single Row of Tubes, *Exp Thermal Fluid Sci ,* **1**, 315-323, 1988
19 Aihara, T , Shimoyama, T , Hongoh, M , and Fujinawa, K., Instrumentation and Error Sources for the Measurement of the Local Drop-Size Distribution by an Immersion-Sampling Cell, *Proceedings,* Third International Conf. on Liquid Atomization and Spray Systems, Institute of Energy, London, Vol. 2, pp VC/5/1-VC/5/11, July 1985.
20. Hiwada, M., and Mabuchi, I , Flow Field and Heat Transfer Around a Circular Cylinder at High Tunnel Blockage Ratios, *Trans Jpn Soc Mech Eng. (Ser B),* **46**, 1750-1759, 1980 (in Japanese)
21 Hiwada, M , Tanba, K , Mabuchi, I., and Kumada, M , Effects of Tunnel Blockage on Local Heat Transfer from a Circular Cylinder in Cross Flow, *Trans Jpn Soc Mech Eng (Ser B),* **42**, 2481-2491, 1976 (in Japanese)
22. Igarashi, T , and Hirata, M , Heat Transfer in Separated Flows (Part 2), *Heat Transfer Jpn Res ,* **6**, 60-78, 1977
23. Zukauskas, A., Heat Transfer from Tubes in Cross Flow, in *Advances in Heat Transfer,* J P. Hartnett and T. E. Irvine, Jr , Eds., Vol 8, pp 93-160, Academic, New York, 1972.
24 Clift, R , Grace, J R , and Weber, M E , *Bubbles, Drops, and Particles,* p 268, Academic, New York, 1978
25. Fujii, T., Kato, Y., and Mihara, K., Expressions of Transport and Thermodynamic Properties of Air, Steam and Water, *Rep. Res Inst. Ind. Sci , Kyushu Univ ,* **66**, 81-95, 1977 (in Japanese).
26 Basilico, C., Jung, G., and Martin, M , Etude du Transfert Convectif Entre un Cylindre Chauffe et un Ecoulement d'Air Charge de Gouttelettes d'Eau, *Int J Heat Mass Transfer,* **24**, 371-385, 1981
27 Aihara, T , Augmentation of Convective Heat Transfer by Gas-Liquid Mist (Keynote Paper), *Proceedings,* 9th International Heat Transfer Conf., Jerusalem, August 1990
28 Aihara, T , Maruyama, S., and Suzuki, Y , Heat and Mass Transfer from a Single Row of Heated Cylinders in Gas-Liquid Mist Flow (General Representation of Heat Transfer Performance), *Proceedings,* 25th National Heat Transfer Symposium of Japan, Kanazawa, Vol 1, pp 187-189, June 1988 (in Japanese)

Received revised April 17, 1990